G-type magnetic order in ferropnictide Cu_{x}Fe_{1−y}As induced by hole doping on As sites

T. Zou, C. C. Lee, W. Tian, H. B. Cao, M. Zhu, B. Qian, C. R. dela Cruz, W. Ku, Z. Q. Mao, and X. Ke

Phys. Rev. B **95**, 054414 — Published 10 February 2017

DOI: 10.1103/PhysRevB.95.054414

G-type magnetic order in ferropnictide $Cu_xFe_{1-y}As$ induced by hole doping to As sites

T. Zou[1], C. C. Lee[2], W. Tian[3], H. B. Cao[3], M. Zhu[1], B. Qian[4,5], C.R. dela Cruz[3], W. Ku[6+], Z. Q. Mao[4], and X. Ke[1*]

[1] *Department of Physics and Astronomy, Michigan State University, East Lansing, MI 48824, USA*

[2] *Institute for Solid State Physics, The University of Tokyo, Kashiwa, Chiba 277-8581, Japan*

[3] *Quantum Condensed Matter Division, Oak Ridge National Laboratory, Oak Ridge, Tennessee 37831, USA*

[4] *Department of Physics and Engineering Physics, Tulane University, New Orleans, Louisiana 70118, USA*

[5] *Advanced Functional Materials Lab and Department of Physics, Changshu Institute of Technology, Changshu 215500, China*

[6] *Department of Physics and Astronomy, Shanghai Jiao Tong University, Shanghai 200240, China*

Strong antiferromagnetic (AFM) correlation has long been postulated to be closely related to the occurrence of unconventional high-temperature superconductivity observed in the cuprates, heavy fermions and organic superconductors. The recently-discovered Fe-based superconductors add another interesting member to the list. However, insufficient attention has been paid to the versatile nature of the magnetic correlation in these materials: some showing stripe (C-type) order, others double stripe (*E*-type) or block AFM order instead, implying potentially richer structures of the superconducting order. Here we report the first observation of yet another AFM correlation in the family: a G-type AFM order as seen in the high-T_c cuprates,

in $Cu_xFe_{1-y}As$ compounds isostructural to the LiFeAs superconductor. This study not only sheds light on the underlying mechanism of the rich magnetic correlations in the Fe-based superconductors, but also suggests the possibility of realizing a distinct pairing symmetry upon chemical doping or applying pressure.

The discovery of high-temperature superconductivity in iron pnictides and chalcogenides (i.e., ferropnictides and ferrochalcogenides) has attracted immense interest [1-12]. One distinct characteristic of ferropnictide and ferrochalcogenide superconductors is that their superconductivity emerges in close proximity to antiferromagnetic (AFM) order, similar to the scenario seen in high-T_c cuprate, heavy-fermion, and organic superconductors [13-15]. This has refueled the long-standing postulation of the deep relationship between AFM correlation and unconventional high-temperature superconductivity [8,10]. Correspondingly, since the discovery of this new member of high-T_c materials, the magnetic correlation has been intensively studied [8,10,16] and various microscopic mechanisms for the magnetic correlation have been heatedly debated [17-19], but no consensus has been reached.

In sharp contrast to the simple G-type antiferromagnetic (AFM) insulating state in the cuprate superconductor parent compounds [20] (Fig. 1a), the parent compounds of Fe-based superconductors exhibit much more complex magnetic behavior and metallic electronic structure. First, the ferropnictides, including 1111 (RFeAsO, R = La, Ce …) [5,9,11,12], 122 (AFe_2As_2, A = Ba, Sr, Ca and K) [2,6,21-23], and 111 (AFeAs, A = Na) families [24], possess a single-stripe, collinear C-type AFM order (Fig. 1b). Second, the parent compound of the "11" ferrochalcogenide family, i.e. $Fe_{1+x}Te$, shows a double-stripe AFM order (Fig. 1c) [25]. Even more, ferrochalcogenide $A_2Fe_4Se_5$ (A = K, Rb, Cs, Tl) ("245") is found to host a block checkerboard AFM order (Fig. 1d) [26,27], adding further complexity to the magnetism of ferrochalcogenides and ferropnictides.

Such a rich variety of magnetic structures poses a great challenge to the basic understanding of their mechanism. For instance, with the *same* nesting vector of the electronic Fermi surface observed in all ferropnictides and ferrochalcogenides, the standard picture of spin

density wave of itinerant magnetism [28-30] cannot account for all the magnetic structures discussed above for the different wave-vectors they correspond to. And while the distinct magnetic structures in these materials can be fitted with highly anisotropic next-neighboring (NN) couplings in conjunction with the strongly material-sensitive next-nearest neighbor (NNN) interactions [16,23], such a strong anisotropy and material dependence is hard to be rationalized from the spin channel alone. Instead, it likely results from coupling to the itinerant carriers and other degrees of freedom, for example the orbital order [31]; or more specifically, it has been proposed that the complex interplay of the kinetic energy of degenerate itinerant carriers and the potential energy of local moments can produce all three magnetic structures [32].

In this paper, we report a surprising discovery of yet another magnetic correlation in $Cu_xFe_{1-y}As$, a "111" type iron pnictide: a collinear G-type AFM order below the Neel temperature T_{N1} = 220 K followed by a canted AFM state below T_{N2} = 140 K to (Fig. 1e and 1f). Such magnetic states are sharply contrasted with the previously-reported single- and double-stripe AFM orders for the "1111", "122", "111" and "11" systems, or the block checkerboard AFM order for the "245" system, but bears some similarity with the magnetic structure of cuprate superconductor parent compounds. However, unlike the insulating G-AFM state in cuprates, the G-AFM/canted G-AFM state in $Cu_xFe_{1-y}As$ comes with metallic transport properties. Such magnetic states offer us important additional clues and constraints to understand the mechanism of magnetic correlation of these families of materials. Our *ab initio* electronic structure calculations indicate that Cu vacancies in this material give rise to hole doping to As sites, leading to spin polarization of As p_x and p_y orbitals. This mediates additional NNN ferromagnetic (FM) coupling and promotes the formation of the G-AFM order. Our findings advocate the active role of the anions and imply the necessity to take into account of their

orbital/spin polarization beyond the previous consideration of just their height [32]. Furthermore, the new magnetic correlation is expected to host a different pairing symmetry if superconductivity can be induced via doping or applying pressure in future explorations.

CuFeAs crystallizes into a Cu_2Sb type tetragonal structure with a space group of P4/nmm at room temperature. Earlier studies [33,34] have found that CuFeAs is non-superconducting down to 2 K, though it is isostructural to Fe-based superconductors NaFeAs and LiFeAs [24,35-37]. The reported magnetic properties of this material are controversial. CuFeAs was initially reported as a material showing FM - like behavior with the Curie temperature $T_c \sim 40$ K [33], while Thakur *et al.* claimed that this material is AFM with a Néel temperature of 9 K based on magnetic susceptibility measurements [34]. Recent studies by Qian *et al.* on single crystal Cu_xFeAs have found that it exhibits weak ferromagnetism below $T_c \sim 42$ K [38]. Moreover, they also found that Cu sites have vacancies with the Cu content being in the 0.62 - 0.73 range. Given that CuFeAs shares similar crystal structure with the "111" family of Fe-based superconductors, it is of fundamental importance to clarify its magnetic properties and unite it with the magnetism of other Fe-based superconductor parent compounds.

Single crystals of CuFeAs were synthesized using self-flux method [38]. The actual composition of the sample used in this study is also nonstoichiometric, i.e. $Cu_{0.68}Fe_{0.80}As$ [39]. Thus we will use the $Cu_xFe_{1-y}As$ formula to represent our sample hereafter. Fig. 2(a) displays the temperature dependence of the heat capacity of $Cu_xFe_{1-y}As$, from which two anomalies can be seen. The first anomaly occurs at $T \sim 220$ K, which has not been reported in previous studies [33,34,38,39]. The second anomaly, which is much weaker than the one near 220 K, occurs near 63 K. This can be attributed to the presence of the weak ferromagnetism arising from spin canting in the AFM state as discussed below.

The temperature evolution of magnetic susceptibility of $Cu_xFe_{1-y}As$ is shown in Fig. 2(b). It was measured during warming with 1000 Oe magnetic field applied along the in-plane and out-of-plane directions after a zero field cooling (ZFC) process, respectively. One can see a dramatic increase in magnetic moment around 63 K, which suggests the onset of the weak FM state, a feature similar to what was reported previously [38]. The small cusp in the specific heat at 63 K can be associated with the occurrence of this weak ferromagnetism. In addition, the material exhibits magnetic anisotropy with the spin easy-axis lying in the *ab* plane.

To understand the nature of the anomaly shown in the heat capacity around 220 K and reveal the intrinsic magnetic ground state of this system, we have performed comprehensive neutron and synchrotron x-ray diffraction measurements [39]. Unlike the tetragonal-to-orthorhombic structural phase transition in other ferropnictides (e.g., NaFeAs [24]), we have found no indication of a potential structural distortion upon cooling [39]. Therefore, one can reasonably infer that the specific heat anomaly near 220 K for $Cu_xFe_{1-y}As$ is most likely associated with the onset of magnetic ordering. Our neutron scattering measurements demonstrate that this is the case. Fig. 3(a) shows the rocking curve scan at Q = (0 0 0.5) at different temperatures. We observed a remarkable Bragg peak at 4 K; this peak becomes extinct at T = 150 K and 250 K indicating its magnetic nature. The temperature dependence of the (0 0 0.5) neutron scattering intensity is presented by the blue symbols in Fig. 3(c) where one can see that the (0 0 0.5) magnetic reflection disappears around 140 K, consistent with the absence of magnetic Bragg scattering intensity beyond the background signal measured at 150 K (Fig. 3a). This feature implies a magnetic phase transition occurring with $T_{N2} \sim 140$ K, which is much lower than the temperature (220 K) associated with the strong anomaly shown in the heat

capacity measurement (Fig. 2a). Surprisingly, we found no anomaly around this temperature in the heat capacity data.

To resolve these puzzles, we examined the temperature dependence of another magnetic Bragg peak at (1 0 0.5). As we will show later, the non-zero intensity of the (0 0 0.5) and (1 0 0.5) Bragg peaks at 4 K likely originates from two different types of magnetic structures. Fig. 3(b) shows the rocking curves of (1 0 0.5) measured at different temperatures. Interestingly, unlike the (0 0 0.5) peak, the (1 0 0.5) peak sustains to high temperature; a noticeable scattering intensity near (1 0 0.5) can still be seen at 150 K, though it is much weaker than that measured at 4 K. This implies that at 150 K, $Cu_xFe_{1-y}As$ is in an AFM state with a distinct magnetic structure from that at 4 K. The extinction of neutron scattering intensity at (1 0 0.5) above 220 K, as shown in Fig. 3(c) and Fig. 3S in [39], suggests that this material becomes AFM below $T_{N1} \sim 220$ K, consistent with the specific heat measurement (Fig. 2a). The magnetic entropy is likely released mostly at T_{N1} such that the specific heat anomaly at T_{N2} becomes non-observable as shown in Fig. 2(a).

The unusual temperature dependences of the (1 0 0.5) and (0 0 0.5) neutron scattering intensity described above imply different magnetic structures for temperature regions below and above T_{N2}, which are indeed revealed by the representational analysis using the BasIrreps program in FULLPROF [39,40]. For $T < T_{N2}$, a canted spin structure (Fig. 1e) with a FM component along the in-plane direction (*a* or *b*-axis) and an AFM component along the *c*-axis was resolved. The spin canting angle is ~ 50º relative to the *c*-axis and the magnetic moment is 0.18(1) μ_B/Fe. We note that small ordered moments are also observed in other FeAs - based compounds such as NaFeAs and LaOFeAs [9,24], the possible origin of which is the high itinerancy of charge carriers [41]. Given that $Cu_xFe_{1-y}As$ shows quasi-two-dimensional metallic

transport properties, it is not surprising to lead to small ordered moments. The in-plane FM component arising from the spin canting in the AFM state revealed in our experiments accounts for the previously reported weak ferromagnetism in $Cu_xFe_{1-y}As$ [38]. In contrast, for $T_{N2} < T < T_{N1}$, the AFM state should feature a typical G-type order without spin canting (Fig. 1f), which is evidenced by the fact that the (1 0 0.5) magnetic peak is present, while the (0 0 0.5) peak is absent. Unfortunately, the scattering intensity of magnetic Bragg peaks other than the (1 0 0.5) peak above T_{N2} is not convincingly measurable above the background due to the very small intensity, which prevents us from determining exactly the spin direction.

The G-type AFM structure in $Cu_xFe_{1-y}As$ implies antiferromagnetic NN interaction and weaker AFM (or potentially FM) NNN interaction, which is in contrast to other ferropnictides. To explore the underlying mechanism that gives rise to this unusual G-type order, we have performed first-principles calculations [39]. The resulting band structure of CuFeAs in Fig. 4(a) shows clearly that (green dressed) Cu *d* bands are deep below the chemical potential. That is, Cu atoms are in the Cu^+ configuration with fully filled *d* orbitals and are thus magnetically inert. Therefore, decreasing Cu concentration dopes hole carriers into the Fe-As layers. One might thus be tempted to believe that in the heavily hole doped case $Cu_{1-x}FeAs$, Fe atoms can lose one electron to behave like Mn and promote G-type AFM order [42].

However, our detailed analysis indicates that a novel mechanism involving orbital/spin polarization of As atoms is in action here. For simplicity and clarity, Fig. 4(c) (d) and (e) show the spin resolved partial density of states (DOS) of As p_x orbital and band structure plots of a heavily hole doped $Cu_{1-x}FeAs$ with $x = 1$. Fig. 4(c) shows clearly a significant enhancement of the As-p_x DOS above the Fermi level (vertical line at zero energy) in the down-spin channel, indicating that a large portion of the doped hole carriers reside in the As p_x orbital [defined in

Fig. 4(b)] which makes this orbital strongly spin polarized and magnetic active. The same is illustrated in more detail by the magenta dressed components of As p_x orbital in Fig. 4(d) and (e). We illustrate in Fig. 4(b) the basic features found in our numerical study. Since the As p_x orbital couples strongly (antiferromagnetically) to the two NNN Fe atoms, it naturally promotes the microscopic processes that mediate FM coupling between them. Similarly, with doped holes the p_y orbital couples to the other two neighboring Fe atoms as well. In the presence of AFM NN coupling, it is easy to see that such a NNN FM process favors G-type over the more common C-type magnetic order in the typical Fe-based superconductors, and consequently the As atom develops an unusual orbital-dependent spin texture shown in Fig. 4(b). One thus expects a strong tendency towards G-type magnetic order against the A-type order upon lowering the Cu concentration. Indeed, our DFT calculation of $Cu_{1-x}FeAs$ shows the correct qualitative trend in the total energy against the C-type order with the G-type about 253 meV more energetically favorable in $Cu_{1-x}FeAs$ at $x = 1$ than at $x = 0$. While the calculations were done on systems with stoichiometric Fe, the Fe vacancy sites of our studied compound will very likely be filled by the slightly smaller Cu^{1+} ion and thus only weaken the magnetic order via dilution of spin moments. This should not change the local correlation or long range order between Fe ions.

Finally, note from Fig. 4(b) that Fe atoms also tend to possess a staggered orbital order when having more hole carriers in alternating d_{xz} and d_{yz} orbitals. The system can further lower its energy (at $T < T_{N2}$) by additional symmetry breaking via, for example, the charge order and new orbital ordering. This would introduce uneven magnitudes in magnetic moments, consistent with the observed canted magnetic pattern.

Now back to the pnictide families, the G-type AFM order reported here is the first case for ferropnictides. This weakly ordered metallic state of Fe d^6 configuration is also to be

distinguished from the previously reported G-type AFM in $BaMn_2As_2$ [42], in which the high-spin d^5 configuration of Mn atoms gives a much larger ordered moment of 3.88 μ_B/Mn and an insulating state. Realization of this new structure of correlation offers additional clues and constraints to the intensively studied and still debated microscopic mechanisms of magnetic correlation in iron-based superconducting materials, and calls for the necessity of revisiting the roles of anion sites in addition to the previously proposed anion height in understanding the mechanism of local magnetic correlations [32]. Furthermore, given that a superconducting state involves pairing of carriers of specific spin texture [8,10,16], having a new magnetic correlation in this family implies a new superconducting pairing symmetry in iron based compounds [17-19], if superconductivity can be induced via chemical doping or external pressure in future explorations. A contrasting case like that would be highly valuable in revealing the intrinsic nature of the superconductivity in the Fe-based superconductors, and help to resolve the long-standing puzzle of high-temperature unconventional superconductivity in general.

In summary, we reported a surprising discovery of a G-type antiferromagnetic order in $Cu_xFe_{1-y}As$, adding a new member to the already rich magnetic correlations in the ferropnictide and ferrochalcogenide families. We have shown that this newly unraveled magnetic correlation arises from hole-doping to As sites due to Cu vacancies, which leads to spin polarization of As *p* orbitals that mediates additional ferromagnetic next-nearest-neighbor interactions. The finding of this distinct magnetic correlation not only provide valuable contrast that gives additional clues and constraints to the existing competing pictures of magnetic correlation in these materials, but also offer potential opportunities to realize superconductivity of different pairing symmetry in ferrochalcogenides and ferropnictides in future explorations.

X. K. acknowledges support from the start-up funds at Michigan State University. The work at Tulane (i.e. $Cu_xFe_{1-y}As$ single crystal growth and characterization) is supported by the U.S. Department of Energy under EPSCoR Grant No. DE-SC0012432 with additional support from the Louisiana Board of Regents. Research conducted at ORNL's High Flux Isotope Reactor was sponsored by the Scientific User Facilities Division, Office of Basic Energy Sciences, US Department of Energy. B. Q. is supported by National Natural Science Foundation of China (Grants No. 11374043, 11174043, and 51371004), Natural Science Foundation of Jiangsu Educational Department (Grant No. 13KJA430001) and six-talent peak of Jiangsu Province (Grants No. 2011-XCL-022 and No. 2012-XCL- 036). W. K. acknowledges support from National Natural Science Foundation of China (Grant No. 11447601) and Ministry of Science and Technology (Grant No. 2016YFA0300500 and 2016YFA0300501).

* ke@pa.msu.edu

+ weiku@mailaps.org

Figure captions:

Figure 1. (a) G-type antiferromagnetic structure, (b) Collinear single-stripe antiferromagnetic structure, (c) Double-stripe antiferromagnetic structure. The red and blue arrows indicate the spin direction of Fe atoms in (a), (b) and (c). (d) Block checkboard antiferromagnetic structure, with the open squares representing the Fe vacancy while + and – symbol representing the spin direction of Fe atoms pointing to opposite directions along the c-axis. Magnetic structure of $Cu_xFe_{1-y}As$ determined by neutron diffraction at 4 K (e) and 150 K (f), respectively. The spin direction at 150 K could not be uniquely determined due to the limitation of the data obtained.

Figure 2. (a) Specific heat of $Cu_xFe_{1-y}As$ as a function of temperature measured during cooling from 250 K to 2 K. The two purple arrows at 220 K and 63 K correspond to the antiferromagnetic and weak ferromagnetic transitions, respectively. Inset shows an expanded view. (b) Magnetic susceptibility of $Cu_xFe_{1-y}As$ measured with 1000 Oe magnetic field applied along both in plane and out of plane directions after zero field cooling.

Figure 3. Rocking scan of the Q = (0 0 0.5) (a) and Q = (1 0 0.5) (b) magnetic Bragg reflections at 4 K, 150 K and 250 K. The neutron counting time is 30 s and 480 s, respectively. (c) The temperature profile of the peak intensities of the Q = (0 0 0.5) and (1 0 0.5) magnetic Bragg peaks with the counting time of 180 s and 600 s, respectively. The dark blue and pink curves are guides to the eyes.

Figure 4. (a) Electronic band structure of G-type CuFeAs with highlighted Cu-d orbital component, showing clearly that they are well below the Fermi energy (at zero) and fully occupied. (b) Illustration of strong next-nearest-neighbor ferromagnetic coupling of Fe atoms bridged by the spin-polarized p_x or p_y orbital of the As atom in the G-type antiferromagnetic

configuration. (c) Comparison of the As p_x partial density of states for $x = 0$ and $x = 1$ in G-type order, showing a large enhancement of down-spin component above the Fermi level upon reduction of Cu (highlighted by the green circle). (d) and (e), The band structure for the case of $x = 1$, with highlighted As p_x contribution showing a strong spin polarization.

Figure 1.

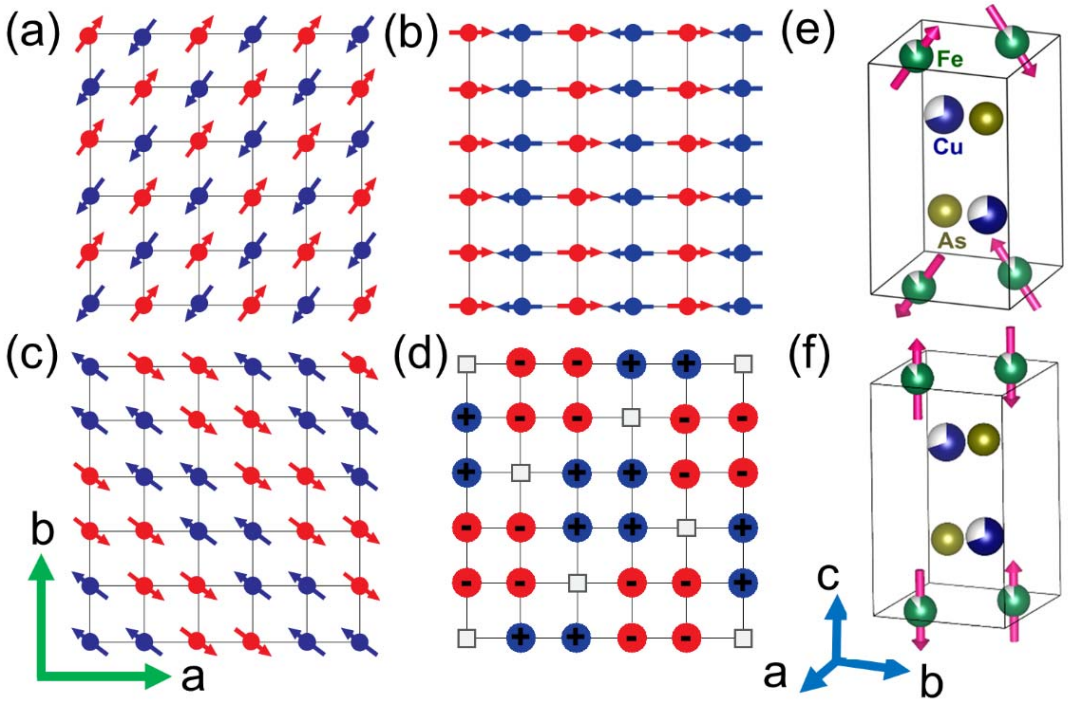

Figure 2.

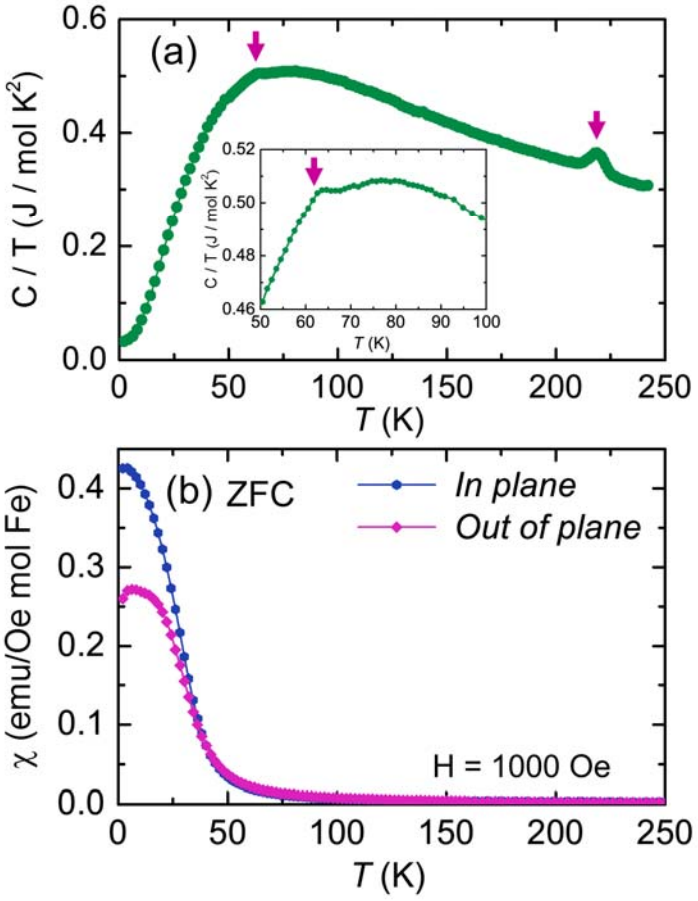
(a)
C / T (J / mol K^2)
T (K)
(b) ZFC
In plane
Out of plane
H = 1000 Oe
χ (emu/Oe mol Fe)
T (K)

Figure 3.

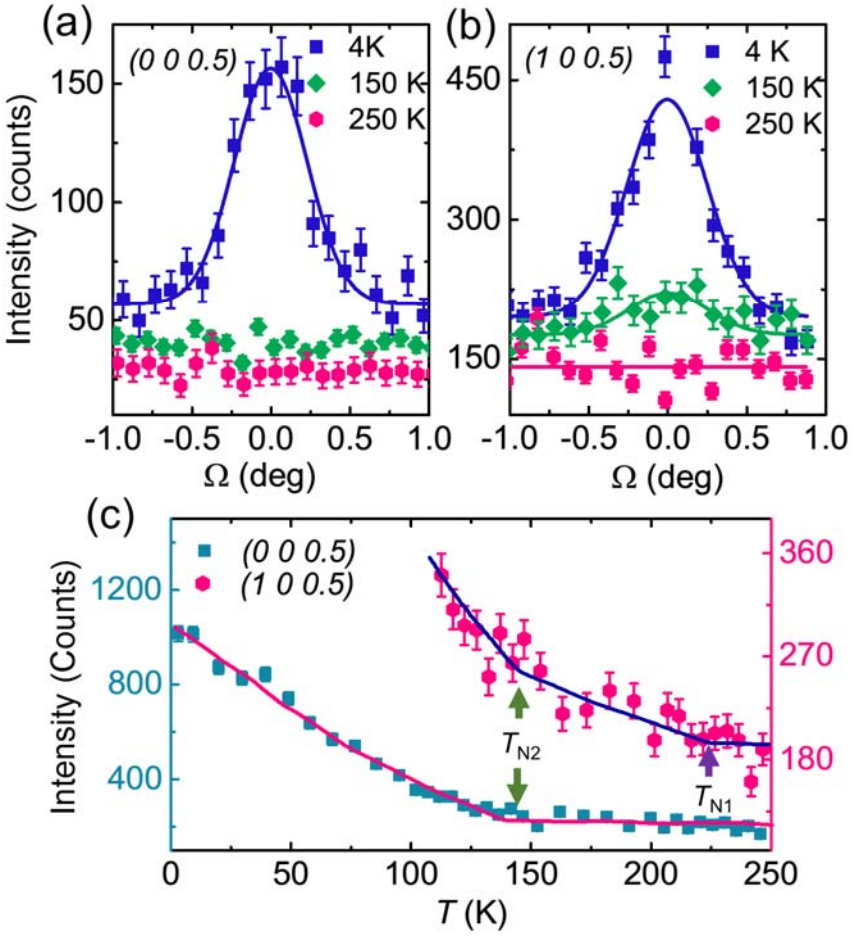
(a)
(0 0 0.5)
4K
150 K
250 K
Intensity (counts)
150
100
50
-1.0 -0.5 0.0 0.5 1.0
Ω (deg)
(b)
(1 0 0.5)
4 K
150 K
250 K
450
300
150
-1.0 -0.5 0.0 0.5 1.0
Ω (deg)
(c)
(0 0 0.5)
(1 0 0.5)
Intensity (Counts)
1200
800
400
360
270
180
T_{N2}
T_{N1}
0 50 100 150 200 250
T (K)

Figure 4.

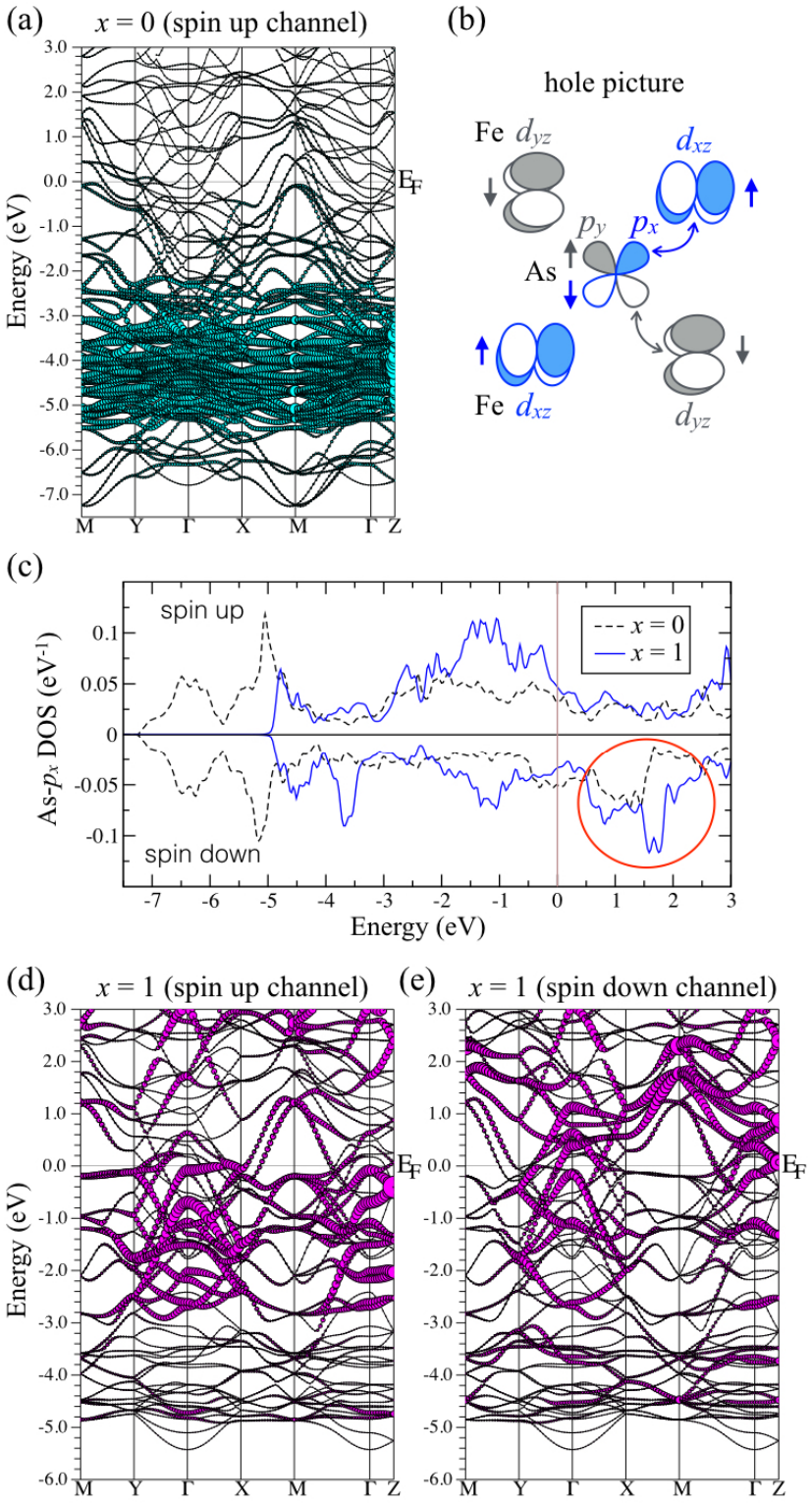
(a)
x = 0 (spin up channel)
Energy (eV)
E_F
M Y Γ X M Γ Z
(b)
hole picture
Fe d_yz
d_xz
p_y
p_x
As
Fe d_xz
d_yz
(c)
spin up
spin down
x = 0
x = 1
As-p_x DOS (eV^-1)
Energy (eV)
(d)
x = 1 (spin up channel)
(e)
x = 1 (spin down channel)

References:

1 Yoichi Kamihara, Takumi Watanabe, Masahiro Hirano, and Hideo Hosono, J. Am. Chem. Soc. **130**, 3296 (2008).

2 A. D. Christianson, E. A. Goremychkin, R. Osborn, S. Rosenkranz, M. D. Lumsden, C. D. Malliakas, I. S. Todorov, H. Claus, D. Y. Chung, M. G. Kanatzidis, R. I. Bewley, and T. Guidi, Nature **456**, 930 (2008).

3 Marianne Rotter, Marcus Tegel, Dirk Johrendt, Inga Schellenberg, Wilfried Hermes, and Rainer Poettgen, Phys. Rev. B **78**, 020503 (2008).

4 Hiroki Takahashi, Kazumi Igawa, Kazunobu Arii, Yoichi Kamihara, Masahiro Hirano, and Hideo Hosono, Nature **453**, 376 (2008).

5 Jun Zhao, Q. Huang, Clarina de la Cruz, Shiliang Li, J. W. Lynn, Y. Chen, M. A. Green, G. F. Chen, G. Li, Z. Li, J. L. Luo, N. L. Wang, and Pengcheng Dai, Nat. Mater. **7**, 953 (2008).

6 Q. Huang, Y. Qiu, Wei Bao, M. A. Green, J. W. Lynn, Y. C. Gasparovic, T. Wu, G. Wu, and X. H. Chen, Phys. Rev. Lett. **101**, 257003 (2008).

7 Fong-Chi Hsu, Jiu-Yong Luo, Kuo-Wei Yeh, Ta-Kun Chen, Tzu-Wen Huang, Phillip M. Wu, Yong-Chi Lee, Yi-Lin Huang, Yan-Yi Chu, Der-Chung Yan, and Maw-Kuen Wu, Proc. Natl. Acad. Sci. U. S. A. **105**, 14262 (2008).

8 G. R. Stewart, Rev. Mod. Phys. **83**, 1589 (2011).

9 Clarina De la Cruz, Q. Huang, J. W. Lynn, Jiying Li, W. Ratcliff Ii, J. L. Zarestky, H. A. Mook, G. F. Chen, J. L. Luo, N. L. Wang, and Pengcheng Dai, Nature **453**, 899 (2008).

10 Pengcheng Dai, Jiangping Hu, and Elbio Dagotto, Nat. Phys. **8**, 709 (2012).

11 P. M. Aswathy, J. B. Anooja, P. M. Sarun, and U. Syamaprasad, Supercond. Sci. Technol. **23**, 073001 (2010).

12 V. Sadovskii Mikhail, Phys. Usp. **51**, 1201 (2008).

13 Patrick A. Lee, Naoto Nagaosa, and Xiao-Gang Wen, Rev. Mod. Phys. **78**, 17 (2006).

14 Christian Pfleiderer, Rev. Mod. Phys. **81**, 1551 (2009).

15 Gunzi Saito and Yukihiro Yoshida, Chem. Rec. **11**, 124 (2011).

16 Pengcheng Dai, Rev. Mod. Phys. **87**, 855 (2015).

17 A. V. Chubukov, D. V. Efremov, and I. Eremin, Phys. Rev. B **78**, 134512 (2008).

18 P. J. Hirschfeld, M. M. Korshunov, and I. I. Mazin, Rep. Prog. Phys. **74**, 124508 (2011).

19 Jiangping Hu and Hong Ding, Sci. Rep. **2**, 381 (2012).

20 Y. S. Lee, R. J. Birgeneau, M. A. Kastner, Y. Endoh, S. Wakimoto, K. Yamada, R. W. Erwin, S. H. Lee, and G. Shirane, Phys. Rev. B **60**, 3643 (1999).

21 Marianne Rotter, Marcus Tegel, and Dirk Johrendt, Phys. Rev. Lett. **101**, 107006 (2008).

22 J. Zhao, W. Ratcliff, J. W. Lynn, G. F. Chen, J. L. Luo, N. L. Wang, J. P. Hu, and P. C. Dai, Phys. Rev. B **78**, 4 (2008).

23 Jun Zhao, D. T. Adroja, Dao-Xin Yao, R. Bewley, Shiliang Li, X. F. Wang, G. Wu, X. H. Chen, Jiangping Hu, and Pengcheng Dai, Nat. Phys. **5**, 555 (2009).

24 Shiliang Li, Clarina de la Cruz, Q. Huang, G. Chen, T. L. Xia, J. Luo, N. Wang, and Pengcheng Dai, Phys. Rev. B **80**, 020504(R) (2009).

25 Wei Bao, Y. Qiu, Q. Huang, M. A. Green, P. Zajdel, M. R. Fitzsimmons, M. Zhernenkov, S. Chang, Minghu Fang, B. Qian, E. K. Vehstedt, Jinhu Yang, H. M. Pham, L. Spinu, and Z. Q. Mao, Phys. Rev. Lett. **102**, 247001 (2009).

26 F. Ye, S. Chi, Wei Bao, X. F. Wang, J. J. Ying, X. H. Chen, H. D. Wang, C. H. Dong, and Minghu Fang, Phys. Rev. Lett. **107**, 137003 (2011).

27 Wei Bao, Qing-Zhen Huang, Gen-Fu Chen, M. A. Green, Du-Ming Wang, Jun-Bao He, and Yi-Ming Qiu, Chin. Phys. Lett. **28**, 086104 (2011).

28 Alaska Subedi, Lijun Zhang, D. J. Singh, and M. H. Du, Phys. Rev. B **78**, 134514 (2008).

29 Y. Xia, D. Qian, L. Wray, D. Hsieh, G. F. Chen, J. L. Luo, N. L. Wang, and M. Z. Hasan, Phys. Rev. Lett. **103**, 037002 (2009).

30 T. J. Liu, J. Hu, B. Qian, D. Fobes, Z. Q. Mao, W. Bao, M. Reehuis, S. A. J. Kimber, K. Prokeš, S. Matas, D. N. Argyriou, A. Hiess, A. Rotaru, H. Pham, L. Spinu, Y. Qiu, V. Thampy, A. T. Savici, J. A. Rodriguez, and C. Broholm, Nat. Mater. **9**, 718 (2010).

31 Chi-Cheng Lee, Wei-Guo Yin, and Wei Ku, Phys. Rev. Lett. **103**, 267001 (2009).

32 Wei-Guo Yin, Chi-Cheng Lee, and Wei Ku, Phys. Rev. Lett. **105**, 107004 (2010).

33 B. Lv, Ph.D. thesis, University of Houston (2009).

34 Gohil S. Thakur, Zeba Haque, L. C. Gupta, and A. K. Ganguli, J. Phys. Soc. Jpn. **83**, 054706 (2014).

35 C. W. Chu, F. Chen, M. Gooch, A. M. Guloy, B. Lorenz, B. Lv, K. Sasmal, Z. J. Tang, J. H. Tapp, and Y. Y. Xue, Physica C: Superconductivity **469**, 326 (2009).

36 G. F. Chen, W. Z. Hu, J. L. Luo, and N. L. Wang, Phys. Rev. Lett. **102**, 227004 (2009).

37 Joshua H. Tapp, Zhongjia Tang, Bing Lv, Kalyan Sasmal, Bernd Lorenz, Paul C. W. Chu, and Arnold M. Guloy, Phys. Rev. B **78**, 060505(R) (2008).

38 B. Qian, J. Hu, J. Liu, Z. Han, P. Zhang, L. Guo, Xuefan Jiang, Tao Zou, Mengze Zhu, C. R. Dela Cruz, Xianglin Ke, and Z. Q. Mao, Phys. Rev. B **91**, 014504 (2015).

39 Supplementary materials.

40 E. Hovestreydt, M. Aroyo, S. Sattler, and H. Wondratschek, J. Appl. Crystallogr. **25**, 544 (1992).

41 Yu-Ting Tam, Dao-Xin Yao, and Wei Ku, Phys. Rev. Lett. **115**, 117001 (2015).

42 Yogesh Singh, M. A. Green, Q. Huang, A. Kreyssig, R. J. McQueeney, D. C. Johnston, and A. I. Goldman, Phys. Rev. B **80**, 100403 (2009).